Computational Materials Science 115 (2016) 99–103

Contents lists available at ScienceDirect

Computational Materials Science

journal homepage: www.elsevier.com/locate/commatsci

First-principles study of Bi and Al in orthorhombic $PbZrO_3$

Maneerat Chotsawat [a,b], Kanoknan Sarasamak [a,b,c], Pitiporn Thanomngam [a,b,c], Sukit Limpijumnong [d], Jiraroj T-Thienprasert [b,e,*]

[a] College of Nanotechnology, King Mongkut's Institute of Technology Ladkrabang, Chalongkrung Road, Ladkrabang, Bangkok 10520, Thailand
[b] Thailand Center of Excellence in Physics (ThEP Center), Commission on Higher Education, Bangkok 10400, Thailand
[c] Nanotec-KMITL Center of Excellence on Nanoelectronic Devices, King Mongkut's Institute of Technology Ladkrabang, Chalongkrung Road, Ladkrabang, Bangkok 10520, Thailand
[d] School of Physics, Institute of Science, Suranaree University of Technology, Nakhon Ratchasima 30000, Thailand
[e] Department of Physics, Faculty of Science, Kasetsart University, Bangkok 10900, Thailand

ARTICLE INFO

Article history:
Received 26 June 2015
Received in revised form 31 December 2015
Accepted 6 January 2016
Available online 2 February 2016

Keywords:
First-principles calculations
DFT
Orthorhombic $PbZrO_3$
PZO

ABSTRACT

Lead zirconate $PbZrO_3$ (PZO) is one of the most important ceramic materials due to its antiferroelectric property, which can be used in many technological applications. Due to the toxicity of Pb, there is an attempt to replace Pb with other non-toxic elements. It has been reported that doping orthorhombic-PZO with Bi and Al atoms could stabilize the antiferroelectric property in a wide temperature range and reduce the lead content in the material. In this work, we used first-principles calculations based on density functional theory to investigate the microscopic and electronic structures of Bi and Al defects in orthorhombic-PZO. Our calculated defect formation energies revealed that Bi atom can substitute on either Pb site (A-site) or Zr site (B-site); depending on the Fermi-level as well as the crystal growth condition. On the other hand, Al atom is likely to substitute only on the Zr site. In addition, our calculations revealed that there is only a small binding between Bi_{Pb} and adjacent Al_{Zr} or Bi_{Zr} with the binding energies of ~0.2 eV. This indicates that Bi_{Pb} and Al_{Zr} (or Bi_{Zr}) are unlikely to form complexes.

1. Introduction

Lead zirconate $PbZrO_3$ or PZO is a versatile ceramic material discovered more than fifty years ago [1,2]. PZO is used in many technological applications such as actuator, high-energy storage devices, diagnostic materials, and bolometer for thermonuclear reactors [3–9]. PZO can exhibit an antiferroelectric phase or paraelectric phase depending on the temperature. At temperatures below 220 °C, PZO has an orthorhombic perovskite structure with an antiferroelectric character [10,11]. At temperatures above its Curies temperature T_c [12] (230 °C), PZO changes to the cubic perovskite structure with a paraelectric character [11]. In the narrow temperature range of 220–230 °C, PZO is reported to show an intermediate ferroelectric character, which is attributed to the presence of defects [13]. In addition, PZO is one of the major components for preparing the solid solution of lead zirconate titanate ($PbZr_{1-x}Ti_xO_3$ or PZT). In particular, the composition near the so-called morphotropic phase boundary (at $x \approx 0.47$) has the best efficiency PZT, which is used in many electronic devices [14–16]. Due to the toxicity of Pb, research on reducing the Pb content in these materials as well as developing lead-free ferroelectric materials is widely carried out [17,18]. For lead-based materials, it is found to be challenging to maintain the antiferroelectric properties while reducing the Pb content.

Tan et al. [19] proposed that the ferroelectric phase of perovskite oxides can be stabilized by replacing A-site cations with larger ions or B-site cations with the smaller ones. They also proposed that the antiferroelectric phase can be stabilized by replacing A-site cations with smaller ions or B-site cations with larger ones. This means by doping PZO with suitable cations at A- and/or B-sites, one can enhance the antiferroelectric property of PZO and, in some cases, reduce the Pb content as well. In addition, there are several reports on the study of $BiMO_3$ ($M = Fe^{3+}$, Mn^{3+} and Nd^{3+}) as potential multiferroic materials [20–22]. $BiMO_3$–$PbTiO_3$ has also been shown to improve the ferroelectric property of $PbTiO_3$ [23–26]. However, scarce information on $BiMO_3$ with M being non-magnetic ions (M = Al, Sc, or Ga) is available. Bismuth aluminate ($BiAlO_3$ or BAO) is one of an interesting lead-free ferroelectric material due to its high curie temperature of ~530 °C [27,28]. BAO has been predicted to be a high-performance ferroelectric and piezoelectric material due to its noncentrosymmetric structure caused by the Bi lone pair ($6s^2$) [29,30]. Recently, Vittayakorn and

* Corresponding author at: Department of Physics, Faculty of Science, Kasetsart University, Bangkok 10900, Thailand.
E-mail addresses: sukit@sut.ac.th (S. Limpijumnong), fscicwt@ku.ac.th (J. T-Thienprasert).

http://dx.doi.org/10.1016/j.commatsci.2016.01.002
0927-0256/

Boonchom reported that the incorporation of BAO into PZO could stabilize the antiferroelectric phase of PZO in a wide temperature range [31]. The stability of the antiferroelectric phase was attributed to the substitution of Pb^{2+} by Bi^{3+} and Zr^{4+} by Al^{3+}. To our knowledge, there is no theoretical work to support these experimental results.

In this paper, we use first-principles density functional calculations to systematically study Bi and Al defects in orthorhombic-PZO. The stability and structure of Bi and Al defects in PZO, under different crystal growth conditions (from O-rich to O-poor), can be obtained based on the defect formation energy. This work provides a deeper understanding on the preferential sites for Bi and Al atoms in orthorhombic-PZO, which is a crucial foundation to explain the antiferroelectric state observed in the BAO–PZO systems.

2. Computational methods

We used first-principles calculations based on density functional theory (DFT) within the local density approximations (LDA) as implemented in the Vienna ab-initio Simulation Package (VASP) [32–34]. The electron–ion interactions were described by the projector augmented wave (PAW) method [35] and the cutoff energy for expanding the plane-wave basis set was set to 500 eV. For the calculations with the 40-atom orthorhombic-PZO unit cell, the Monkhorst–Pack scheme [36] with a sampling k-point mesh of $3 \times 3 \times 3$ was used for the k-space integrations. The calculated lattice constants of orthorhombic-PZO are $a = 5.837$ Å, $b = 11.723$ Å and $c = 8.131$ Å. These calculated values are in agreement with the experimental results [37]. To study Bi and Al defects in PZO, the supercell approach was employed [38–40] with the 80-atom orthorhombic-PZO supercell, which is a $2 \times 1 \times 1$ repetition of the 40-atom unit cell. For the supercell calculations the sampling k-point mesh was reduced to $2 \times 2 \times 2$. All atoms in the supercell were allowed to relax until the Hellmann–Feynman forces [41] acting on each atom became less than 0.02 eV/Å. The likelihood of defect formation, such as a Bi substitution for Pb (Bi_{Pb}) or Zr (Bi_{Zr}) atom, could be determined from the defect formation energy defined by [39]

$$E_f(D^q) = E_{tot}(D^q) - E_{tot}(0) - \sum_x n_x \mu_x + E_{corr} + q(E_F + E_{VBM}), \quad (1)$$

where $E_{tot}(D^q)$ is the total energy of a supercell containing the defect D in charge state q and $E_{tot}(0)$ is the total energy of the defect-free supercell, n_x is the number of atom species x (x can be Pb, Zr, O, Bi or Al atom), being added to a supercell to create the defect D in charge state q with the corresponding atomic chemical potential μ_x (discussed next), E_{corr} is the finite-size correction term for charged defects according to the scheme proposed by Freysoldt et al. [42,43], and E_F is the Fermi level referenced to the valence band maximum (VBM). Lower defect formation energy means that the defect is more likely to form.

Under thermodynamic equilibrium, to slowly grow a high quality orthorhombic-PZO crystal, the following conditions must be satisfied,

$$E_{tot}(PbZrO_3) = \mu_{Pb} + \mu_{Zr} + 3\mu_O, \quad (2)$$

where $E_{tot}(PbZrO_3)$ is the total energy per formula unit of orthorhombic-PZO and μ_{Pb}, μ_{Zr}, and μ_O are atomic chemical potentials for Pb, Zr, and O atoms, respectively. If the sum on the right-hand side of Eq. (2) is much larger than the left-hand side, the crystal will be rapidly and ununiformly grown. On the other hand, if the sum on the right-hand side is smaller than the left-hand side, the crystal will disintegrate. These atomic chemical potentials can be any values lying on a plane according to Eq. (2). In order to prevent the phase precipitation, such as metallic and O_2 gas phases, μ_{Pb}, μ_{Zr}, and μ_O are then limited by the total energy per formula unit of metallic Pb, metallic Zr, and O_2 gas, respectively, *i.e.*,

$$\mu_{Pb} < E_{tot}(\text{Pb-metal}), \quad \mu_{Zr} < E_{tot}(\text{Zr-metal}), \quad \text{and } \mu_O < E_{tot}(O_2)/2. \quad (3)$$

Consequently, the plane determined by Eq. (2) is limited to a triangle plane restricted by Eq. (3). In addition, Pb and Zr atoms could form the oxide phases such as PbO and ZrO_2. To prevent such precipitation phases, the following conditions must be taken into consideration,

$$\begin{aligned} &\mu_{Pb} + \mu_O < E_{tot}(PbO), \quad \mu_{Pb} + 2\mu_O < E_{tot}(PbO_2), \\ &3\mu_{Pb} + 4\mu_O < E_{tot}(Pb_3O_4), \quad \mu_{Zr} + \mu_O < E_{tot}(ZrO), \\ &\mu_{Zr} + 2\mu_O < E_{tot}(ZrO_2). \end{aligned} \quad (4)$$

By solving Eqs. (2)–(4), we could determine the chemical potentials for Pb, Zr, and O as depicted in Fig. 1. In Fig. 1, all chemical potentials were referenced to their natural phases, *i.e.*, metallic Pb, metallic Zr, and O_2 gas. The lines connecting the points A–B, B–C and C–A are limited by ZrO_2, metallic Pb, and Pb_3O_4 phases, respectively. The chemical potentials for Pb, Zr and O can assume any set of values, represented by a point on the plane depicted in Fig. 1. As shown in Eq. (1), the defect formation energy is a function of the chemical potentials. For convenience, we choose to present the defect formation energies under two crystal growth conditions, *i.e.*, O-rich and O-poor growth conditions. When incorporating Bi and Al into PZO, we need to ensure that there is no phase precipitation produced by Bi and Al, such as metallic Bi, metallic Al, BiO_2, and Al_2O_3. We found that for O-poor growth condition μ_{Bi} and μ_{Al} are limited by E_{tot}(Bi-metal) and $[E_{tot}(Al_2O_3) - 3\mu_O]/2$, respectively, while μ_{Bi} and μ_{Al} are restricted by $[E_{tot}(Bi_2O_3) - 3\mu_O]/2$ and $[E_{tot}(Al_2O_3) - 3\mu_O]/2$ for O-rich growth condition.

3. Results and discussion

Fig. 2 illustrates a 80-atom supercell of orthorhombic-PZO in which there are two inequivalent Pb atoms (Pb_1 and Pb_2) alternately arranged on a plane perpendicular to the c-axis. An orthorhombic-PZO is a slight distortion from the perfect cubic perovskite structure by tilting of the oxygen octahedral [44]. To study the microscopic and electronic structures of Bi and Al defects in orthorhombic-PZO, we calculated the formation energies associated with Bi and Al defects, which are explicitly a function of oxygen chemical potential as explained in the previous section. The

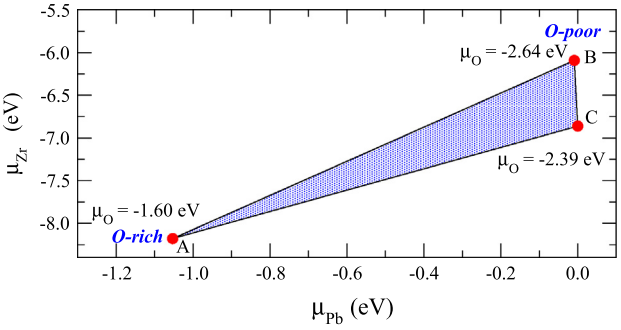

Fig. 1. Illustration of the possible range of Pb, Zr, and O chemical potentials for the thermodynamic equilibrium growth of $PbZrO_3$. The three dimension plot is reduced into two dimension plot by projecting oxygen chemical potential onto Pb–Zr plane. The red points represent the chemical potential for oxygen at the boundaries according to Eqs. (2)–(4). All values of the atomic chemical potentials are referenced to their natural phases, *i.e.*, Pb-metallic, Zr-metallic, and O_2 gas. (For interpretation of the references to colour in this figure legend, the reader is referred to the web version of this article.)

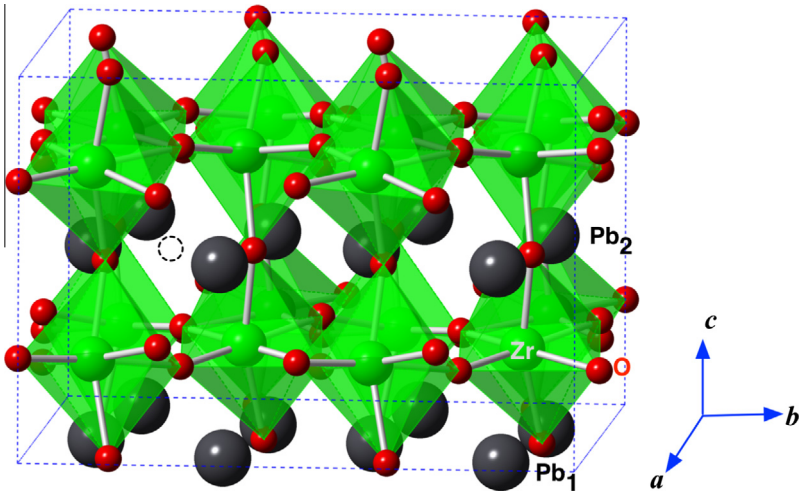

Fig. 2. Illustration of the 80-atom supercell of orthorhombic-$PbZrO_3$. The black, green, and red colours represent Pb, Zr, and O atoms, respectively. The dashed circle indicates an interstitial site for Bi and Al atoms. There are two inequivalent Pb atoms, labeling as Pb_1 and Pb_2, that are alternately arranged on a plane perpendicular to the *c*-axis. (For interpretation of the references to colour in this figure legend, the reader is referred to the web version of this article.)

formation energies are shown for two extreme growth conditions, *i.e.*, O-rich and O-poor growth conditions and the chemical potentials of Bi and Al are set to their highest possible values before the phase precipitations are taken place as described in the previous section. Note that, the formation energy plots for other conditions can be obtained by referring to Eq. (1). Because our calculation is based on the LDA functional, the VBM and CBM positions are known to contain some errors. This directly affects the calculated formation energy as shown in the last term of Eq. (1). To remedy this problem, we performed additional calculations with hybrid functional proposed by Heyd–Scuseria–Ernzerhof (HSE06) with the mixing parameter of 0.25 to determine the more reliable VBM and CBM positions. Our HSE calculations give the band gap of 3.98 eV, which is only slightly larger than the experimental band gap of 3.70 eV [45]. It is also believed that the calculation with HSE functional gives more accurate VBM and CBM positions than LDA. To correct our calculated formation energy obtained from LDA calculations, we need to align the VBM positions obtained from LDA (VBM_{LDA}) and HSE (VBM_{HSE}) functionals with respect to the vacuum level to determine the offset between them ($\Delta_{LDA-HSE}$) [46]. This could be accomplished by performing a slab calculation as described in Ref. [47]. Here, we constructed a (001)-surface of orthorhombic-PZO with a 10-layer slab separated by a vacuum region. All atoms in the outermost three layers were allowed to relax while the remaining atoms were kept fixed to represent the bulk-like region. We found that VBM_{LDA} is 0.44 eV higher than VBM_{HSE}, *i.e.*, $\Delta_{LDA-HSE}$ = 0.44 eV. To apply the correction, we rigidly shifted the VBM_{LDA} in Eq. (1) by $\Delta_{LDA-HSE}$, *i.e.*, we replace E_{VBM} by $E_{VBM} + \Delta_{LDA-HSE}$. This results in the left-shift of the VBM position in the formation energy plot by 0.44 eV. To illustrate this shift, the position of VBM_{LDA} without the correction is shown using a vertical dashed line in Fig. 3. (The correction effectively moved down the VBM by 0.44 eV.)

In Fig. 3, the formation energies of A-site substitutions (X_{Pb}), B-site substitutions (X_{Zr}), and interstitial defects (X_i), where *X* can be Bi or Al atom, are shown. The Fermi energy is plot from 0 (referenced to the VBM) up to the experimental band gap (~3.70 eV). Note that the calculated band gap at the Γ-point is only 2.64 eV, which is smaller than the experimental band gap of 3.70 eV [45] due to the well-known DFT underestimation of the band gap. Our calculations (with actual charge occupations) are possible without populating the (calculated) conduction band because the special *k*-point band gap in the supercell calculation is larger than 3.7 eV. For Bi substitutional defects, we found that the formation energy of Bi_{Pb} at the Pb_2's site is slightly lower (by 0.07 eV) than that at the Pb_1's site. Bi_{Pb} is a single donor defect with a defect transition level $\varepsilon(+1/0)$ = 3.58 eV. Bi_{Zr} is an amphoteric defect with a defect transition level $\varepsilon(+1/-1)$ = 1.45 eV. From the plot, it is clear that the formation energy of Bi_{Pb} is lower than that of Bi_{Zr} when the Fermi level is less than 1.78 eV and 2.30 eV for O-rich and O-poor growth conditions, respectively. At higher Fermi level, the formation energy of Bi_{Zr} turns lower. Therefore, Bi can substitute on both Pb's and Zr's sites depending on the Fermi level and the crystal growth condition. For Bi_i defect, we found that Bi atom prefers to occupy the vacant site lying on the Pb_2 plane as illustrated in the dashed circle in Fig. 2. Bi_i is a donor with a defect transition level $\varepsilon(+3/+1)$ = 2.60 eV with a negative-*U* behavior. Its formation energy is higher than the substitutional defects; indicating that Bi atom is likely to exist in the form of substitutional defect in orthorhombic-PZO rather than the interstitial defect. Regarding Al substitutional defects, we found that Al_{Pb} at Pb_1's site is slightly lower in energy (by 0.08 eV) than that at Pb_2's site. Al_{Pb} is a shallow donor, while Al_{Zr} is a shallow acceptor. Both Al_{Pb} and Al_{Zr} defects do not create any defect level inside the band gap. The formation energy of Al_{Zr} becomes lower than that of Al_{Pb} when the Fermi level is above 0.71 eV and 1.23 eV for O-rich and O-poor growth conditions, respectively. For Al_i defect, it is a triple shallow donor without any defect transition level and it locates at the same site as Bi_i defect. Its formation energy is high but turns lower at the Fermi levels near the VBM. Note that the interstitial defects (Bi_i and Al_i) are triple donors (3+ charge state) which means the formation energy after Makov–Payne correction would significantly increased; making them more difficult to form. Although, they have low formation energy when the PZO sample has the Fermi level near the VBM, once they are formed, they will quickly shift the Fermi level of the system higher; suppressing further formation. Therefore, these interstitial defects would not form in a substantial amount.

From Fig. 3, we can see that the leading donor and acceptor are Bi_{Pb} and Al_{Zr}, respectively. They pin the Fermi energy of the system (where the formation energy of the leading donor and acceptor crossed) at ~1.6 and 2.2 eV for O-rich and O-poor growth conditions, respectively. Earlier study of native point defects in orthorhombic-PZO [48] showed that the leading native donor and acceptor are oxygen vacancy (V_O) and lead vacancy (V_{Pb}), respectively. They are double donor and double acceptor, respec-

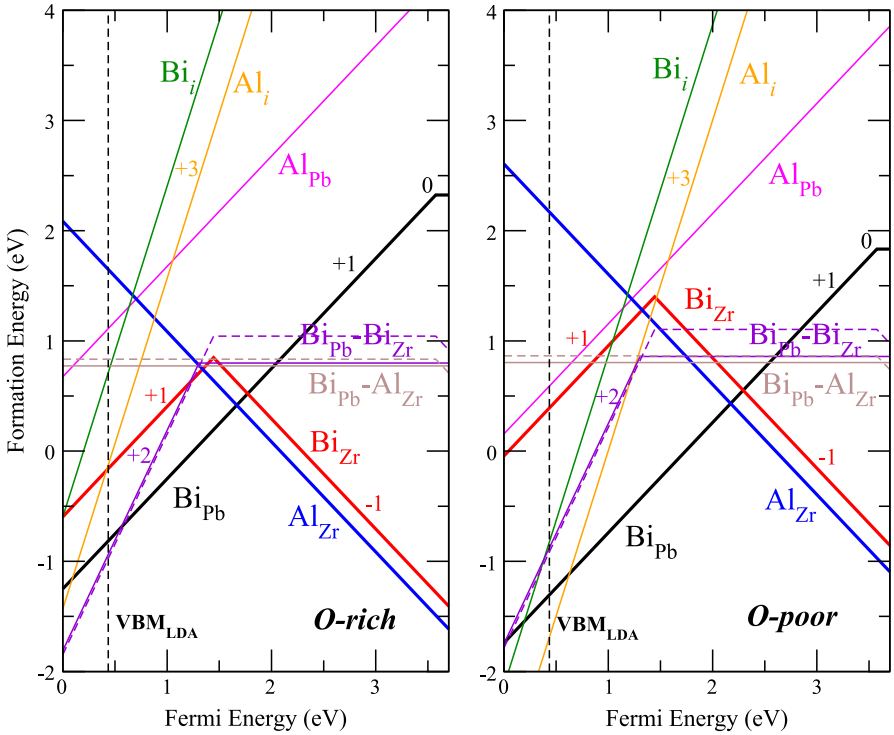

Fig. 3. Defect formation energies (after corrected by referencing to HSE VBM) as a function of Fermi energy under O-rich (left) and O-poor (right) growth conditions. The slope of each line represents the charge state of the defect. The Fermi energy is extended to the experimental band gap of ~3.70 eV. The dashed lines represent the sums of the formation energies of isolated defects, *i.e.*, Bi_{Pb} + Bi_{Zr} (purple) and Bi_{Pb} + Al_{Zr} (brown). The vertical dashed line indicates position of the LDA VBM before corrected by the HSE calculations. (For interpretation of the references to colour in this figure legend, the reader is referred to the web version of this article.)

tively. Their formation energies increase twice as fast compared to the single donor (Bi_{Pb}) and single acceptor (Al_{Zr}) as the Fermi level shifts away from the band edge toward the mid gap. As a result, native defects are not the leading donor or leading acceptor when Bi and Al are present. Interestingly, if PZO is doped only with Bi (i.e., no Al), the leading donor and acceptor are Bi_{Pb} and Bi_{Zr}, respectively. This means Bi is a self-compensating impurity. It can substitute for Pb and behave as a donor and can substitute for Zr and behave as an acceptor under a given growth condition. Therefore, the general belief that, in BAO–PZO systems, Bi and Al could substitute for only their best fitted site, should be revised.

Table 1 showed the crystal ionic radii of Pb^{2+}, Zr^{4+}, O^{2-}, Bi^{3+}, and Al^{3+}. The ionic radius of Bi is smaller than that of Pb, but is larger than that of Zr. The radius of Al is the smallest of all elements listed. This is consistent with our calculated results that Bi atom can substitute for both Pb and Zr sites, whereas Al atom prefers to substitute only for Zr site. According to Tan et al. [19], if one replaces A-site with a smaller ion (compared to Pb) or B-site with a larger ion (compared to Zr), it should stabilize the antiferroelectric properties of PZO. In this case, the substitution of Bi on the A-site (Bi_{Pb}) as well as the substitution of Bi on the B-site (Bi_{Zr}) would help stabilizing antiferroelectric properties. However, for Al atom, which has the smallest ionic radius, when it is placed on the B-site, Al_{Zr} should effectively destabilize the antiferroelectric property of PZO [19]. Because the experimental results showed that co-doping PZO with both Bi and Al helps stabilizing the antiferroelectric property in a wide temperature range [31], the effect of Bi on stabilizing the antiferroelectric property must be more pronounced than the destabilizing effect of Al. Because Bi atom could substitute for both Pb and Zr atoms; acting as single donors and single acceptors, respectively, they can self-compensate without the need of Al. We, therefore, propose that doping PZO with only Bi atom under proper growth conditions, that allow self-compensation, can be more beneficial to the antiferroelectric property than co-doping with both Bi and Al atoms.

Table 1
Ionic radii in picometers (pm) for Pb^{2+}, Zr^{4+}, O^{2-}, Bi^{3+}, and Al^{3+} [49].

Ion	Pb^{2+}	Zr^{4+}	O^{2-}	Bi^{3+}	Al^{3+}
Ionic radii (pm)	133	86	126	117	67.5

Next, we investigated the likelihood of complex formation between the donor (Bi_{Pb}) and acceptors (Bi_{Zr} or Al_{Zr}). We calculated Bi_{Pb}–Al_{Zr} and Bi_{Pb}–Bi_{Zr} complex defects. To determine the stability of such complex defects, we calculated the binding energy of such complex defects defined by

$$E_{\text{bind}}(A-B) = E_f(A) + E_f(B) - E_f(A-B), \quad (5)$$

where $E_f(A)$ and $E_f(B)$ are the formation energies of defects A and B, and $E_f(A-B)$ is the formation energy of the A–B complex defect. If the complex has a large binding energy, it is more likely to form. As shown in Fig. 3, the calculated binding energy of Bi_{Pb}–Al_{Zr} and Bi_{Pb}–Bi_{Zr} complexes are small (i.e., 0.06 eV and 0.24 eV, respectively). This is consistent with the fact that Bi_{Pb} is a shallow donor and Al_{Zr} (as well as Bi_{Zr}) is a shallow acceptor. Majority of Bi and Al atoms in orthorhombic-PZO should be in the form of isolated substitutional defect.

4. Conclusions

By using first-principles calculations, we investigated the microscopic and electronic structures of Bi and Al defects in orthorhombic-PZO. The stability of each defect is evaluated by calculating its formation energy. Our calculated results revealed that Bi atom could substitute not only on the Pb site (A-site), but also on the Zr site (B-site); depending on the Fermi-level as well as the

crystal growth condition. The substitution of Bi on either site would help stabilizing antiferroelectric property of PZO. On the other hand, Al atom is likely to substitute only on the Zr site (B-site) and destabilizing antiferroelectric property of PZO. Because Bi can serve as a donor (when substitute for Pb) and an acceptor (when substitute for Zr), it can be self-compensated without the need of Al to co-doped. We propose that doping PZO with only Bi, under proper growth conditions, can better stabilizing antiferroelectric property than when co-doping with Al. The study of donor–acceptor complex pairs between Bi_{Pb} and Bi_{Zr} or Al_{Zr} reveals that the complexes are bound with low binding energies ($\sim$0.1 to 0.2 eV). The majority of Bi and Al atoms in orthorhombic-PZO should exist in the form of isolated substitutional defects.

Acknowledgements

This research was supported by Thailand Research Fund (TRG5780259), Kasetsart University Research and Development Institute (M-V13.57 and V-T(D)49.58), and Faculty of Science, Kasetsart University (RFG 1-4). We would like to acknowledge the Synchrotron Light Research Institute (SLRI), Thailand for the computational resources.

References

[1] E. Sawaguchi, Ferroelectrics 266 (2002) 341–353.
[2] H. Fujishita, Ferroelectrics 266 (2002) 27–40.
[3] S.S. Sengupta, D. Roberts, J.F. Li, M.C. Kim, D.A. Payne, J. Appl. Phys. 78 (1995) 1171–1177.
[4] K. Yamakawa, S. Trolier-McKinstry, J.P. Dougherty, S.B. Krupanidhi, Appl. Phys. Lett. 67 (1995) 2014–2016.
[5] J.H. Jang, K.H. Yoon, H.J. Shin, Appl. Phys. Lett. 73 (1998) 1823–1825.
[6] B. Xu, P. Moses, N.G. Pai, L.E. Cross, Appl. Phys. Lett. 72 (1998) 593–595.
[7] B. Xu, Y. Ye, L.E. Cross, J. Appl. Phys. 87 (2000) 2507–2515.
[8] R. Seveno, H.W. Gundel, S. Seifert, Appl. Phys. Lett. 79 (2001) 4204–4206.
[9] R. Bittner, K. Humer, H.W. Weber, K. Kundzins, A. Sternberg, D.A. Lesnyh, D.V. Kulikov, Y.V. Trushin, J. Appl. Phys. 96 (2004) 3239–3246.
[10] E. Sawaguchi, H. Maniwa, S. Hoshino, Phys. Rev. 83 (1951) 1078.
[11] D. Viehland, Phys. Rev. B. 52 (1995) 778–791.
[12] S. Wirunchit, N. Vittayakorn, J. Appl. Phys. 104 (2008) 024103–024106.
[13] L. Pintilie, K. Boldyreva, M. Alexe, D. Hesse, J. Appl. Phys. 103 (2008) 024101.
[14] B. Jaffe, W.R. Cook, H. Jaffe, Piezoelectric Ceramics, Academic Press, London/New York, 1971.
[15] Y.L. Du, L.X. Chen, Y.Q. Lei, M.S. Zhang, Rare Metal Mat Eng. 32 (2003) 91–94.
[16] D. Wang, R.B. Yu, S.H. Feng, W.J. Zheng, R.R. Xu, Y. Matsumura, M. Takano, Chem. Lett. 32 (2003) 74–75.
[17] Y. Saito, H. Takao, T. Tani, T. Nonoyama, K. Takatori, T. Homma, T. Nagaya, M. Nakamura, Nature 432 (2004) 84–87.
[18] N. Hajime, Y. Masaki, M. Yoichi, T. Tadashi, Jpn. J. Appl. Phys. 42 (2003) 7401.
[19] Q. Tan, Z. Xu, D. Viehland, J. Mat. Res. 14 (1999) 4251–4258.
[20] C.M. Fernandez-Posada, H. Amorin, C. Correas, O. Pena, M. Alguero, A. Castro, J. Mater. Chem. C. 3 (2015) 2255–2265.
[21] J.A. McLeod, Z.V. Pchelkina, L.D. Finkelstein, E.Z. Kurmaev, R.G. Wilks, A. Moewes, I.V. Solovyev, A.A. Belik, E. Takayama-Muromachi, Phys. Rev. B. 81 (2010).
[22] C.C. Chou, C.L. Huang, S. Mukherjee, Q.Y. Chen, H. Sakurai, A.A. Belik, E. Takayama-Muromachi, H.D. Yang, Phys. Rev. B. 80 (2009).
[23] E.E. Richard, A.R. Clive, R.S. Thomas, W.R. Paul, H. Wes, P. Seung-Eek, Jpn. J. Appl. Phys. 40 (2001) 5999.
[24] C.J. Stringer, T.R. Shrout, C.A. Randall, I.M. Reaney, J. Appl. Phys. 99 (2006).
[25] M.R. Suchomel, P.K. Davies, J. Appl. Phys. 96 (2004) 4405–4410.
[26] M.R. Suchomel, P.K. Davies, Appl. Phys. Lett. 86 (2005).
[27] P. Baettig, C.F. Schelle, R. LeSar, U.V. Waghmare, N.A. Spaldin, Chem. Mater. 17 (2005) 1376–1380.
[28] J. Zylberberg, A.A. Belik, E. Takayama-Muromachi, Z.-G. Ye, Chem. Mater. 19 (2007) 6385–6390.
[29] N.A. Hill, K.M. Rabe, Phys. Rev. B. 59 (1999) 8759–8769.
[30] R. Seshadri, N.A. Hill, Chem. Mater. 13 (2001) 2892–2899.
[31] N. Vittayakorn, B. Boonchom, J. Alloys Compd. 509 (2011) 2304–2310.
[32] L. Hedin, B.I. Lundqvist, J. Phys. C. 4 (1971) 2064.
[33] W. Kohn, L.J. Sham, Phys. Rev. 140 (1965) A1133–A1138.
[34] G. Kresse, J. Hafner, Phys. Rev. B. 47 (1993) 558–561.
[35] P.E. Blöchl, Phys. Rev. B. 50 (1994) 17953–17979.
[36] H.J. Monkhorst, J.D. Pack, Phys. Rev. B. 13 (1976) 5188–5192.
[37] F. Jona, G. Shirane, F. Mazzi, R. Pepinsky, Phys. Rev. 105 (1957) 849–856.
[38] C.G. Van De Walle, J. Neugebauer, J. Appl. Phys. 95 (2004) 3851–3879.
[39] J.E. Northrup, S.B. Zhang, Phys. Rev. B. 50 (1994) 4962–4964.
[40] S.B. Zhang, S.H. Wei, A. Zunger, Phys. Rev. B. 63 (2001) 075205.
[41] R.P. Feynman, Phys. Rev. 56 (1939) 340–343.
[42] C. Freysoldt, J. Neugebauer, C.G. Van de Walle, Phys. Status Solidi B 248 (2011) 1067–1076.
[43] C. Freysoldt, J. Neugebauer, C.G. Van de Walle, Phys. Rev. Lett. 102 (2009).
[44] S.E. Reyes-Lillo, K.M. Rabe, Phys. Rev. B. 88 (2013).
[45] M.P. Moret, M.A.C. Devillers, K. Worhoff, P.K. Larsen, J. Appl. Phys. 92 (2002) 468–474.
[46] A. Alkauskas, A. Pasquarello, Phys. Rev. B. 84 (2011).
[47] P.G. Moses, M.S. Miao, Q.M. Yan, C.G. Van de Walle, J. Chem. Phys. 134 (2011).
[48] M. Chotsawat, K. Sarasamak, P. Thanomngam, J. T-Thienprasert, Integr. Ferroelectr. 156 (2014) 86–92.
[49] R. Shannon, Acta Crystallogr., Sect. A. 32 (1976) 751–767.